Finding the best trajectory of robot-CT using the projection quality and reconstructability

Seungjun Yoo, Seokwon Oh, Junho Lee, Seongbon Park, and Ho Kyung Kim*
Computational X-ray Imaging Laboratory, School of Mechanical Engineering, Pusan Nat'l Univ., 2, Busandaehak-ro 63beon-gil, Busan 46241
**Corresponding author: hokyung@pusan.ac.kr*

***Keywords : Robotic arm, Computed tomography, Trajectory optimization, Data completeness, Metal artifact reduction**

1. Introduction

Computed tomography (CT) reconstructs data acquired from various directions into three-dimensional volumetric images, enabling the visualization of an object's internal structure. Due to this advantage, CT is widely used in both medical and industrial applications for detecting diseases and structural defects. However, unlike in medical imaging, industrial CT inspections often face challenges when scanning large objects that may exceed the system's field of view or objects predominantly composed of metal, which can cause severe metal artifacts and degrade image quality. To address these issues, methods such as scanning only a portion of the object or avoiding regions with high attenuation can be applied. However, these approaches are fundamentally constrained by conventional cone-beam CT (CBCT) systems, which are mostly limited to circular scanning trajectories.

Recently, an alternative approach has been explored to overcome these limitations by mounting an X-ray source and detector on a six-degree-of-freedom (6-DOF) robotic arms, allowing projection acquisition along arbitrary trajectories [1]. While robot-CT systems provide the advantage of acquiring projections from diverse angles, the optimal scanning trajectory remains a black box. In particular, when only a portion of the object is scanned, data completeness may be compromised, leading to degraded image reconstruction quality.

In this study, we propose an optimized trajectory design for robot-CT systems that maximizes data completeness within a specified volume of interest (VOI) while reducing metal artifacts, even with a limited number of projections.

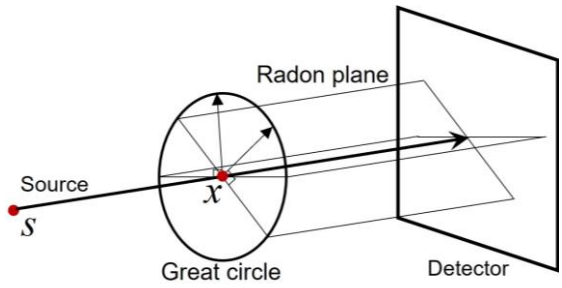

Fig. 1. Sketch of the measuring Radon plane and great circle.

2. Materials and Methods

2.1. Data completeness

In CT, data completeness is a fundamental requirement for exact reconstruction. Tuy [2] and Smith [3] established several conditions, known as Tuy-Smith condition, based on assumptions for exact reconstruction: 1) the scanning trajectory must exist entirely outside the object, 2) the scanning trajectory must be closed, continuous, and mostly differentiable, and 3) any plane passing through the object must intersect the scanning trajectory at least at one point. A Radon plane is a plane defined in the Radon transform, containing specific projection data from within the object. As shown in Fig. 1, when a plane integral is taken from a single source position ***s*** to a single point **x**, the normal vectors of the Radon planes form a great circle. By measuring data from all angles, additional great circles are formed, eventually generating a so-called Radon sphere. A complete Radon sphere indicates that the Radon data is

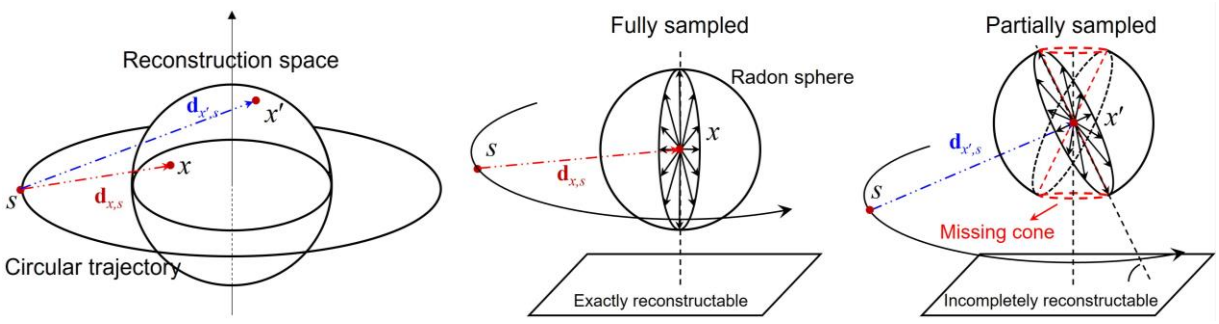

Fig. 2. Examples of local data completeness in CBCT geometry based on conventional circular trajectory.

complete, enabling exact reconstruction. If some Radon planes do not intersect with the source trajectory, it means that those Radon planes are not measured. Consequently, the Radon sphere is not fully formed, and as the number of such unmeasured planes increases, accurate reconstruction becomes increasingly challenging.

Based on the Tuy-Smith condition, Maier et al. [4] defined local data completeness and provided an example of CBCT based on a circular trajectory, as shown in Fig. 2. In this example, **x** is a point located on the trajectory plane, while **x**′ is positioned above the trajectory plane. For **x**, a great circle perpendicular to the trajectory plane is formed, and by combining the great circles obtained from each source point, the Radon sphere is constructed, allowing for accurate reconstruction of any point located on the trajectory plane. However, for **x**′, the measured great circles are tilted, leading to the formation of a missing cone in the Radon data acquired from all trajectory points. As a result, not all necessary projection data are obtained. This missing data explains why distortions like cone beam artifacts in CBCT are more prominent in slices farther from the central slice.

2.2. Trajectory optimization

To quantitatively evaluate data completeness, we employed a Tuy-based measure [4,5]. Let $\mathbf{u}\in\mathbb{R}^3$ be the normal vector of any great circle on the Radon sphere and $\mathbf{d}\in\mathbb{R}^3$ be the normal vector of a measured great circle. The angle γ between these two circles is given by:

$$\gamma = \cos^{-1}|\mathbf{d}^T\mathbf{u}|, \tag{1}$$

where the vector **d** represents the directional vector connecting the source $\boldsymbol{s}$ and the position of the image voxel **x** or VOI being measured for data completeness: $\mathbf{d}(\mathbf{x},\boldsymbol{s}) = \frac{\mathbf{x}-\boldsymbol{s}}{\|\mathbf{x}-\boldsymbol{s}\|_2}$. If γ = 0, it indicates that the measured projection has sampled that great circle. To compute the angle γ, we generated vectors **u** on the unit sphere at uniform angular gap Δα. Similarly, basic source locations were generated on a sphere with a radius equal to the source-to-object distance (SOD). For each **u**, the source location that results in γ = 0 or minimizes γ was selected to construct the trajectory

$$\boldsymbol{s}_i^* = \underset{s}{\operatorname{argmin}}\{\cos^{-1}(|\mathbf{d}(\mathbf{x},\boldsymbol{s})^T\mathbf{u}_i|)\}. \tag{2}$$

When measuring data completeness for a VOI rather than a singe voxel, we first compute $\mathbf{d}(\mathbf{x}_j,\boldsymbol{s}) = \frac{\mathbf{x}_j-\boldsymbol{s}}{\|\mathbf{x}_j-\boldsymbol{s}\|_2}$ for each $\mathbf{x}_j$ within the VOI. Then, for a given $\mathbf{u}_i$, we compute $\cos^{-1}\left(\left|\mathbf{d}(\mathbf{x}_j,\boldsymbol{s})^T\mathbf{u}_i\right|\right)$ for each $\mathbf{x}_j$ and average over all voxels in the VOI:

$$\bar{f}(\boldsymbol{s},\mathbf{u}_i) = \frac{1}{N}\sum_{j=1}^{N}\cos^{-1}\left(\left|\mathbf{d}(\mathbf{x}_j,\boldsymbol{s})^T\mathbf{u}_i\right|\right), \tag{3}$$

where *N* is the number of voxels in the VOI. Finally, the optimal source position $\boldsymbol{s}_i^*$ is determined by minimizing $\bar{f}(\boldsymbol{s},\mathbf{u}_i)$:

$$\begin{aligned}\boldsymbol{s}_i^* &= \underset{s}{\operatorname{argmin}}\{\bar{f}(\boldsymbol{s},\mathbf{u}_i)\}\\ &= \underset{s}{\operatorname{argmin}}\{\tfrac{1}{N}\textstyle\sum_{j=1}^{N}\cos^{-1}\left(\left|\mathbf{d}(\mathbf{x}_j,\boldsymbol{s})^T\mathbf{u}_i\right|\right)\}.\end{aligned} \tag{4}$$

The Tuy-based measure is fully object-independent, requiring additional steps to mitigate metal artifacts in the VOI. After the initial trajectory selection process based on the Tuy-based measure, additional screening was applied to reduce metal artifacts in the VOI. Any projection in which the transmittance of the VOI-projected region was lower than *t* % was excluded.

2.3. Simulation

To validate the trajectory selection algorithm, we conducted MATLAB simulations. The phantom was generated in a 512 × 512 × 512 format with a voxel size of 0.05 mm. The detector had a resolution of 1024 × 1024, with a pixel size of 0.1 mm. To introduce cone-beam artifacts, the SOD was set to 80 mm, with a magnification factor of 2.5, resulting in a maximum cone angle of approximately 40 degrees. The basic trajectory was constructed as a combination of multiple tilted circular trajectories. The rotation angle θ ranged from 0° to 360° with a step angle of 2°, while the tilted angles φ were generated from −80° to 90° at 10° intervals, leading to approximately 3200 source locations.

For image reconstruction, both Feldkamp-Davis-Kress (FDK) and adaptive steepest descent–projections onto convex sets (ASD-POCS) [6] algorithms were used. The voxel size in the reconstructed images was set identical to that of the phantom, 0.05 mm.

2.4. Experimental setup

To develop a robot-CT system, instead of a dual-robot setup where the X-ray source and detector are mounted separately on two robotic arms, we integrated a single robotic arm into the laboratory radiography system. As shown in Fig. 3, the robotic arm (RB5-850, Rainbow

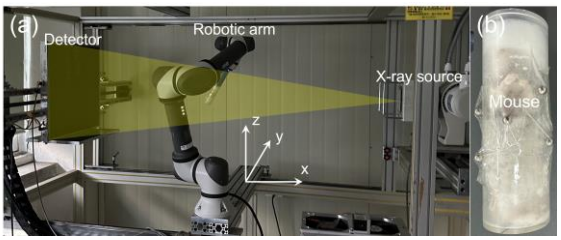

Fig. 3. Experimental setup of the robot-CT system utilizing a single robotic arm: (a) photograph of the system, where the robotic arm holds and rotates the object while the X-ray source and detector remain fixed, (b) mouse phantom

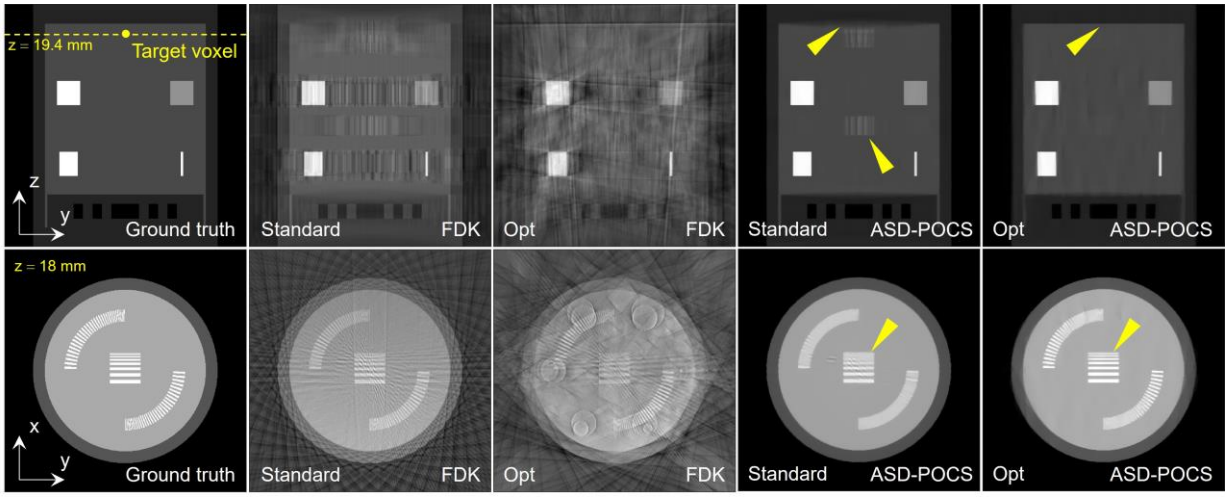

Fig. 4. Comparison of reconstruction results using different trajectories in coronal (top row) and axial (bottom row) views. The ground truth represents the phantom image, while Standard refers to reconstruction using a conventional circular trajectory. Opt denotes the reconstruction obtained with the proposed trajectory optimization method.

Robotics Co., Ltd.) holds and rotates the object at various angles to acquire projections. The X-ray source (E7239X, Toshiba Co., Japan) employs a tungsten target and operates at 70 kV and 10 mA, with an exposure time of 10 ms. Additionally, a 2 mm aluminum was used to filter the X-ray spectrum. The flat-panel detector (FDX4343R, Toshiba Co., Japan) has a resolution of 3072 × 3008 pixels, with a pixel size of 0.143 mm. The SOD was set to 1 m, resulting in an approximate magnification factor of 2. For projection acquisition, a mouse sample was used, with 5 mm metal balls attached around it to induce metal artifacts. The projections were acquired over a rotation range θ of 0° to 360° at 2° intervals, while tilted angles φ of 0°, 30°, and 45° were used, resulting in a total of 540 projections. Image reconstruction was performed using FDK.

3. Preliminary results

3.1. simulation analysis

To validate the proposed trajectory optimization algorithm, a simulation study was conducted. To measure data completeness, vectors **u** were generated with an angular gap $\Delta\alpha$ of 20°, resulting in a total of 62 vectors. The data completeness calculation was performed for a single voxel, the center voxel in the z = 19.4 mm slice. To mitigate cone-beam artifacts, a voxel located farther from the center slice was selected. For each **u**, the source position that yielded the smallest γ was selected, resulting in an initial set of 62 source positions. After removing redundancy, a total of 46 source positions were finalized. The reconstruction using the circular trajectory (standard) was also performed with the same number of projections as the optimized trajectory. In this case, no additional screening for metal artifact reduction was performed. The reconstruction results are presented in Fig. 4.

In the coronal view, when using FDK, both trajectories produced suboptimal image quality, with the optimized trajectory yielding even poorer results. This is because the FDK algorithm is an analytic method based on continuous functions and is particularly well-suited for circular trajectories. Therefore, to better accommodate arbitrary trajectories, we additionally considered ASD-POCS, which is one of algebraic reconstruction techniques. In the ASD-POCS, the optimized trajectory demonstrates a reduction in cone-beam artifacts and additional artifacts compared to standard trajectory (see the yellow arrows). A similar trend was observed in the axial view results. In particular, the ASD-POCS with the optimized trajectory showed improved resolution in the bar pattern.

3.2. measurements

Fig. 5 presents the projection data acquired from the mouse phantom and the corresponding reconstruction results obtained using the FDK algorithm for each tilted angle and the optimized trajectory. In this case, data completeness was evaluated at a selected VOI slice, ensuring that the chosen slices contained metal artifacts for all tilted angles (0°, 30°, and 45°). For vector **u** generation, an angular gap of 10° was used, resulting in a total of 224 vectors. After applying the trajectory optimization algorithm, redundancy was removed, reducing the number of projections from 224 to 180. Additionally, to further reduce metal artifacts, source positions where the transmittance was below 10% were excluded, leading to a final optimized trajectory with 42 source locations. For comparison, the tilted angle reconstructions at 0°, 30°, and 45° were also performed using the same number of projections. In Fig. 5, the top-

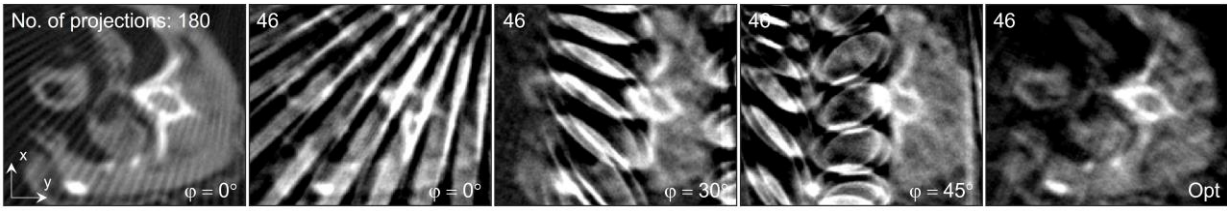

Fig. 5. Axial view reconstruction results of the mouse phantom using different trajectories and number of projections.

left corner of each image indicates the number of projections used for reconstruction, while the bottom-right corner provides information about the corresponding scanning trajectory.

When using a simple tilted circular trajectory, it was difficult to clearly distinguish the cross-sections of the mouse phantom. In contrast, with the optimized trajectory, most of the metal artifacts were significantly reduced. While some data loss is inevitable compared to the case where 180 projections were used at $\varphi = 180°$, the optimized trajectory with only 46 projections was still able to reconstruct most of the internal structures of the mouse. It is expected that by incorporating a greater number of projections from diverse angles and applying trajectory optimization, even better reconstruction results can be achieved.

4. Discussions and Future studies

We departed from conventional circular trajectory-based CBCT by integrating a 6-DOF robotic arm into an existing radiography system, enabling object manipulation at various angles for projection acquisition. To improve image quality, we designed an algorithm based on a Tuy-based measure to quantitatively assess data completeness and identify the optimal trajectory. Compared to the circular trajectory, the optimized trajectory demonstrated enhanced image performance.

In future studies, we aim to further improve the optimization algorithm, transitioning from heuristic approaches to a more global and systematic optimization framework. A more detailed analysis and quantitative evaluation, including the detailed algorithm structure, will be presented and discussed at the conference.

REFERENCES

This work was supported by the National Research Foundation of Korea (NRF) grant funded by the Korea government (MSIT) (RS-2024-00340520).

REFERENCES

[1] W. Holub, F. Brunner, and T. Schön, RoboCT application for in-situ inspection of join technologies of large scale objects, International Symposium on Digital Industrial Radiology and Computed Tomography, 2019.
[2] H. K. Tuy, An inversion formula for cone-beam reconstruction, SIAM Journal on Applied Mathematics, Vol. 43, No. 3, pp. 546-552, 1983.
[3] B. D. Smith, Image reconstruction from cone-beam projections: Necessary and sufficient conditions and reconstruction methods, IEEE Transactions on Medical Imaging, Vol. MI-4, No. 1, pp. 14-25, 1985.
[4] A. Maier, P. Kugler, G. Lauritsch, and J. Hornegger, Discrete estimation of data completeness for 3D scan trajectories with detector offset, Bildverarbeitung für die Medizin 2015.
[5] G. Herl, A. Maier, and S. Zabler, X-ray CT data completeness condition for sets of arbitrary projections, Proc. SPIE 12304, 7th International Conference on Image Formation in X-Ray Computed Tomography, 123040C.
[6] E. Y. Sidky, and X. Pan, Image reconstruction on circular cone-beam computed tomography by constrained, total variation minimization, Physics in Medicine and Biology, Vol. 53, No. 17, pp. 4777-4807, 2008.